# Study on the silicide phase control and room temperature mechanical properties of Nb-Si-Ti based alloys via B and Mg-microalloying

*Dezhi* Chen[1], *Fangdong* Xu[1], *Jingyue* Yu[1], *Shu* Wang[1], *Qi* Wang[1] and *Ruirun* Chen[1*]

[1] National Key Laboratory for Precision Hot Processing of Metals, Harbin Institute of Technology, Harbin 150001, China

**Abstract.** The Nb-16Si-20Ti-4Cr-1.5Al-4Hf-4Zr-1Ta-*x*B (*x*=0, 2, 4)-*y*Mg (*y*=0, 0.2, 0.4) alloys were prepared by non-consumable arc melting. The effects of B and Mg addition on the microstructure and room temperature fracture toughness have been investigated. The results reveal that when the content of B element reached 4 at.%, the intermediate metastable phase $Nb_3Si$ was precipitated in Nb-Si based alloys. The cooperation of B and Mg synergistically enhances the room temperature fracture toughness of Nb-Si based alloy. B and Mg element causes the eutectic point of Nb-Si based alloy to shift to the right. The 2B-0.4Mg alloy shows the best fracture toughness, and its $K_Q$ value is 14.41 MPa·$m^{1/2}$, which increased by 34% compared to the matrix alloy. Crack deflection and secondary cracking increase the room-temperature fracture toughness of Nb-Si-based alloys.

## 1 Introduction

Nb-Si based alloys are considered substitutes for nickel-based superalloys in the aerospace field due to their high service temperatures (1300-1500°C) [1]. Nb-Si based alloys are typically composed of a tough niobium solid solution (Nbss) and hard brittle silicide (Nb5Si3) [2]. Alloying has been widely studied in recent years as an effective means to enhance the mechanical properties of Nb-Si based alloys [3]. However, Nb-Si-based alloys still have a gap from industrial applications due to their poor room temperature fracture toughness [4].

Luo et al. [5] found that the addition of element B has a significant impact on the content of silicide phases. Wu et al. [6] investigated the influence of Mg element on Nb-Si-Ti alloy, revealing that the addition of Mg is beneficial to the compressive strength of the alloy. However, they did not further discuss the strengthening mechanism of Mg. The main purpose of this study is to systematically investigate the combined effects of adding B and Mg elements on the mechanical properties and microstructural evolution of the Nb-Si based alloys, providing an effective pathway for seeking high mechanical performance Nb-Si-based alloys.

* Corresponding author: ruirunchen@hit.edu.cn

## 2 Experiment material and setup

The Nb-16Si-20Ti-4Cr-1.5Al-4Hf-4Zr-1Ta-*x*B (*x*=0, 2, 4)-*y*Mg (*y*=0, 0.2, 0.4) alloys were prepared by non-consumable arc melting. The raw material purity of all alloys in this article is greater than 99.5 wt %. Each ingot is melted at least 6 times to ensure as much uniformity as possible in the chemical composition. The crystal structures were recognized by X-ray diffraction (XRD) with Cu-Kα radiation scanning from 20°to 90° at a rate of 8°/min. Analyzing the microstructure and chemical composition of the sample through scanning electron microscopy (SEM, Merlin compact). The fracture toughness specimen with dimension of 20×4×2 $mm^3$, and the notch depth was 2 mm. Fracture toughness tests were conducted on the testing machine (AG–X Plus 250 kN/50 kN) at a rate of $0.2\times10^{-3}m\times min^{-1}$.

## 3 Results and discussion

### 3.1 Phase constitution microstructure

Fig. 1 shows the diffraction pattern of Nb-16Si-20Ti-4Cr-1.5Al-4Hf-4Zr-1Ta-*x*B (*x*=0, 2, 4) -*y*Mg (*x*=0, 0.2, 0.4) alloys. There are three phases: Nbss, α-$(Nb, X)_5Si_3$ and β-$(Nb, X)_5Si_3$, and no diffraction peaks of $Nb_3Si$ phase in 0B-0Mg alloy. The composition phases of Nb-Si based alloys containing 2 at.% B elements are also Nbss, α-$(Nb, X)_5Si_3$, β-$(Nb, X)_5Si_3$ phases. Nb-Si based alloys with element B content of 4 at.% contain Nbss, α-$(Nb, X)_5Si_3$ and β-$(Nb, X)_5Si_3$ and $Nb_3Si$. It should be noted that the phase composition and diffraction peaks of alloys 2B-0.2Mg and 2B-0.4Mg, as well as alloys 4B-0.2Mg and 4B-0.4Mg, remain basically unchanged, indicating that the influence of Mg element on the phase composition or crystal transformation of silicides is relatively small. The number of α-$(Nb, X)_5Si_3$ phase diffraction peaks in alloys d and e is only two peaks, indicating that the addition of B element to Nb-Si based alloys is the main reason for the appearance of $Nb_3Si$ phase and the disappearance of α-$(Nb, X)_5Si_3$.

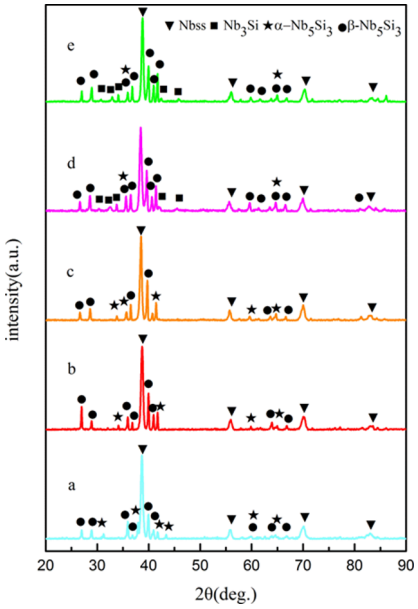


**Fig. 1.** XRD patterns of Nb-16Si-20Ti-4Cr-1.5Al-4Hf-4Zr-1Ta-*x*B (*x*=0,2,4)-*y*Mg (*x*=0,0.2,0.4) alloys: a 0B-0Mg, b 2B-0.2Mg, c 2B-0.4Mg, d 4B-0.2Mg, e 4B-0.4Mg.

Fig. 2 shows the backscattered electron images of Nb-16Si-20Ti-4Cr-1.5Al-4Hf-4Zr-1Ta-*x*B (*x*=0, 2, 4) - *y*Mg (*y*=0, 0.2, 0.4) alloys. Except for the matrix phase, the other four alloys all contain large primary silicide phases, so the matrix phase without B and Mg elements is a fully eutectic alloy, while the Nb-Si based alloys with 2B-0.2Mg, 2B-0.4Mg, 4B-0.2Mg, and 4B-0.4Mg have a hypereutectic structure. This indicates that the eutectic points of Nb-Si based alloys with added elements B and Mg have shifted (towards the direction of high Nb element content), ultimately affecting the microstructure. Adding 2B-0.2Mg and 2B-0.4Mg to the matrix alloy to form α-(Nb, X)$_5$Si$_3$ and β-(Nb, X)$_5$Si$_3$ phase is mostly in the form of long strips, with a relatively flat surface and sharp edges formed at the tips. Its structure undergoes significant damage, forming some incomplete polygons. The silicide phase also "surrounds" some Nbss phases, forming silicides with Nbss phase closure inside. As the temperature decreases, the concentration of Si element changes, and the solubility concentration of Si gradually decreases from the outside to the inside, resulting in the formation of secondary precipitates. Primary silicides are typical polyhedral forms, mainly irregular hexahedral and a few regular hexagonal forms, accompanied by large, pointed silicide phases with strong planar features. This indicates that the eutectic point shifted to the right, resulting in a decrease in Nbss phase generated by the eutectic reaction L→Nb$_3$Si+Nbss. Quantitative analysis was conducted on the proportion of surface area of primary phase silicides, and it was found that the proportions of 2B-0.2Mg, 2B-0.4Mg, 4B-0.2Mg, and 4B-0.4Mg were 7.16%, 10.17%, 7.96%, and 15.93%, respectively. When the Mg element was low at 0.2 at.%, the proportion of silicide phase was relatively small, less than 8%; The Mg content reaches 0.4 at.%, and the proportion of silicide area is relatively high, reaching a maximum of 15.93%, which is nearly twice that of the matrix phase. Based on the above analysis, both B and Mg elements will have an impact on the microstructure. Mg element has a more significant impact on the primary silicide, but B element only increases the precipitation of the primary silicide phase when the Mg content is high.

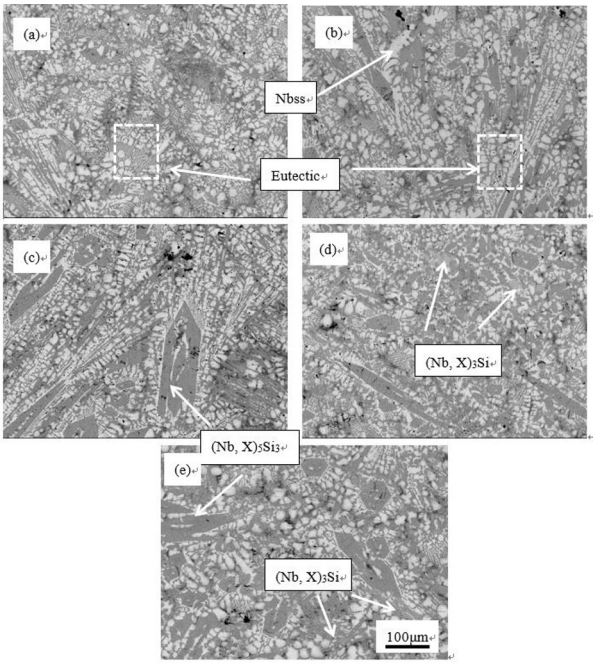


**Fig.2.** BSE images of microstructure of Nb-16Si-20Ti-4Cr-1.5Al-4Hf-4Zr-1Ta-*x*B (*x*=0, 2, 4)-*y*Mg (*y*=0, 0.2, 0.4) alloy: (a) 0B-0Mg, (b) 2B-0.2Mg, (c) 2B-0.4Mg, (d) 4B-0.2Mg, (e) 4B-0.4Mg.

### 3.2 Room temperature fracture toughness

Fig.3 shows the load-displacement curves of the arc-melted Nb-16Si-20Ti-4Cr-1.5Al-4Hf-4Zr-1Ta-*x*B (*x*=0, 2, 4)-*y*Mg (*y*=0, 0.2, 0.4) alloy in the fracture toughness test. Within a displacement of 0.02 mm, the relationship between load and displacement approximated a parabolic shape, indicating better toughness of the material in the initial loading stage. From around 0.02 mm to 0.12 mm, the load and displacement showed a linear relationship, reaching a peak before rapidly dropping, suggesting no significant plastic deformation behavior throughout the room-temperature fracture toughness test. Therefore, it is a typical brittle material.

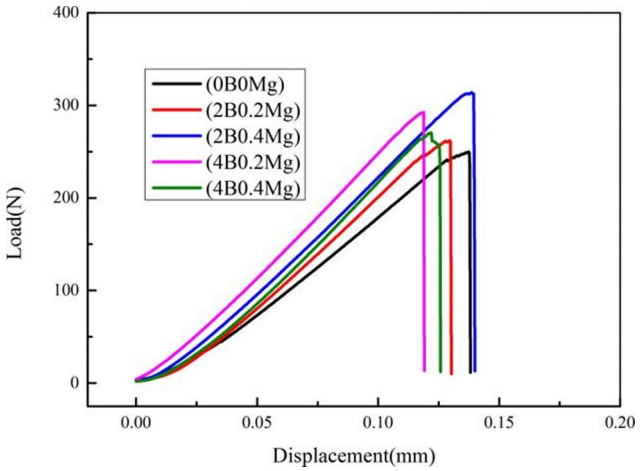


**Fig. 3.** Load-displacement curve of a three-point bending specimen

The fracture toughness values of Nb-Si-based alloys with the addition of 2 at.% B and 0.2 at.% Mg is 12.25 MPa·m$^{1/2}$. As the B content continues to increase, the average $K_Q$ value of the 4B-0.2Mg alloy is 13.51 MPa·m$^{1/2}$, and the $K_Q$ value of the 2B-0.4Mg alloy is the highest at 14.41 MPa·m$^{1/2}$. With further increase in B content, the $K_Q$ value of the 4B-0.4Mg alloy decreases slightly to 13.82 MPa·m$^{1/2}$. This indicates that the addition of an appropriate amount of B element can improve the $K_Q$ value of Nb-Si-based alloys, but the effect on fracture toughness $K_Q$ value is not significant when the B content reaches 4 at.%. This is consistent with the findings of Zhang [7], indicating that the addition of 2 at.% B to Nb-Si-based alloys slightly improves the fracture toughness $K_Q$ value, but the addition of 5 at.% or more B elements leads to a decrease in $K_Q$ value. This may be attributed to two factors: (1) B element affects fracture toughness differently than Zr and Ta elements, introducing interface effects rather than proportional toughness enhancement; (2) excessive B elements promote the precipitation of the metastable phase $Nb_3Si$. In this study, when the B content reaches 4 at.%, the volume fraction of the intermediate phase $Nb_3Si$ is very low, at only 1.54 % and 1.46%, indicating a minor impact of the latter factor. The addition of Mg element can also improve the fracture toughness. When the B element content is low, trace element Mg increases the $K_Q$ value. However, when the B element reaches 4.at%, the influence of Mg element is not significant. This also enhances the bonding strength at the interface. Fig. 4 shows the crack propagation paths of arc-melted Nb-16Si-20Ti-4Cr-1.5Al-4Hf-4Zr-1Ta-*x*B (*x*=0, 2, 4)-*y*Mg (*y*=0, 0.2, 0.4) alloy three-point bending test samples. Overall, the cracks exhibit certain deviations rather than direct through-thickness propagation. After adding 2 at.% B and 0.2 at.% Mg elements, during the crack propagation process, large primary silicide phases were encountered. The cracks propagated along the axis of the silicide, while encountering micro-cracks generated by the silicide phase itself. After a slight extension

along the micro-crack orientation (perpendicular to the axis), the cracks continued to propagate along the axis, encountering a series of micro-cracks. Eventually, a stepped expansion path was formed within the silicide phase. When the Mg content reached 0.4 at.%, the angle of crack deflection significantly increased, and small secondary cracks appeared. A large angle of crack deflection indicates that more energy is absorbed as the crack propagates. In figures (d) and (e), although the deflection angles of the cracks are smaller, crack bridging occurs, and secondary cracks form at voids. In Fig 4(e), a distinct zigzag path is observed as the crack traverses the silicide phase. In the matrix alloy, there are small black areas, which were identified as voids during SEM scanning, indicating the formation of a few defects during solidification in the matrix alloy, thus influencing the overall performance.

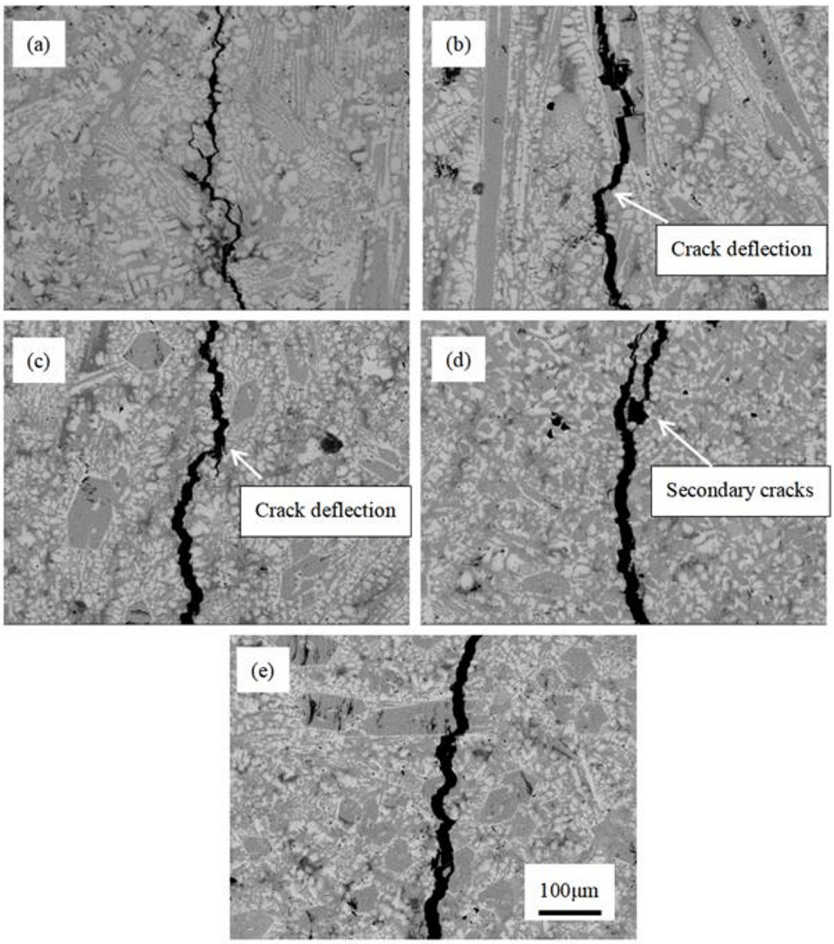


**Fig.4.** Crack propagation path photos of Nb-16Si-20Ti-4Cr-1.5Al-4Hf-4Zr-1Ta-*x*B (*x*=0, 2, 4)-y Mg (*y*=0, 0.2, 0.4) alloy three-point bending test samples.

## 4 Conclusion

In this paper, the effects of B and Mg on the phase formation, microstructure, and fracture toughness of Nb-Si based alloys have been studied, and the following conclusions have been drawn:

1. The addition of 4 at.% B element to Nb-16Si-20Ti-4Cr-1.5Al-4Hf-4Zr-1Ta alloy produces

a metastable phase Nb3Si.

2. B and Mg element causes the eutectic point of Nb-Si based alloy to shift to the right, and the primary silicides increase from 7.10% (2B-0.2Mg) to 15.93% (4B-0.4Mg).

3. The 2B-0.4Mg alloy shows the best fracture toughness, and its KQ value is 14.41 MPa·m1/2. Crack deflection and secondary cracking increase the room-temperature fracture toughness of Nb-Si-based alloys.

This work was supported by the Heilongjiang Postdoctoral Fund (LBH-Z23132) and the China Postdoctoral Science Foundation (2023TQ0099).

## References

1. Q Wang, R Chen, Case Stud. Mater. Sci. Eng. A. **860,** 144223 (2023)
2. Y Qiao, X Guo, Y Zeng, Intermetallics. **88**, 19-27 (2017)
3. Q Wang, C Zhou, S Wang, R Chen, J. Mater. Res. Technol. **9 (6)**, 15585-15592 (2021)
4. X Fang, X Guo, Y Qiao, Intermetallics. **112**, 106798 (2020)
5. L Luo, F Wang, X Meng, Rare Metals **42**, 2801-2808 (2023)
6. M Wu, S Li, L Jiang, PROG NAT SCI – MATER. **21**, 139-145 (2011)
7. S Zhang, X Guo, Intermetallics. **64**, 51-58 (2015)
8. Chan K S, Mater. Sci. Eng. A. **329-331**, 513-522 (2002)
9. M Ashby, F Blunt, M Bannister, Acta Metallurgica. **37**, 1847-1857 (1989)